



High Performance Thick-Film Nonfullerene Organic Solar Cells with Efficiency over 10% and Active Layer Thickness of 600 nm

Yamin Zhang, Huanran Feng, Lingxian Meng, Yanbo Wang, Meijia Chang, Shitong Li, Ziqi Guo, Chenxi Li, Nan Zheng, Zengqi Xie, Xiangjian Wan,* and Yongsheng Chen

Dedicated to the 100th anniversary of Nankai University.

Developing efficient organic solar cells (OSCs) with relatively thick active layer compatible with the roll to roll large area printing process is an inevitable requirement for the commercialization of this field. However, typical laboratory OSCs generally exhibit active layers with optimized thickness around 100 nm and very low thickness tolerance, which cannot be suitable for roll to roll process. In this work, high performance of thick-film organic solar cells employing a nonfullerene acceptor F-2Cl and a polymer donor PM6 is demonstrated. High power conversion efficiencies (PCEs) of 13.80% in the inverted structure device and 12.83% in the conventional structure device are achieved under optimized conditions. PCE of 9.03% is obtained for the inverted device with active layer thickness of 500 nm. It is worth noting that the conventional structure device still maintains the PCE of over 10% when the film thickness of the active layer is 600 nm, which is the highest value for the NF-OSCs with such a large active layer thickness. It is found that the performance difference between the thick active layer films based conventional and inverted devices is attributed to their different vertical phase separation in the active layers.

Solution processed organic solar cells (OSCs) with bulk heterojunction (BHJ) architecture have received intense studies around the world and experienced a dramatic development.^[1–4] Recently, due to the rapid innovation of nonfullerene acceptors (NFAs),^[5–15] a great number of single-junction organic solar cells with power conversion efficiencies (PCEs) over 15%^[16–21] have

been reported. And for tandem solar cells, the PCE has reached 17%.^[22] However, the vast majority of those device performances were obtained with layer-thicknesses at around 100 nm^[23–29] and decreased drastically with the increase of the active layer thickness, which limits their application in the roll to roll large-scale solution printing technology.^[30,31] Furthermore, 20%–40% of the incident photon flux were wasted in such a active layer thickness,^[32] which directly limits the short circuit current density (J_{sc}) of the corresponding OSCs. Thus, it is necessary to develop high efficiency OSCs with tolerance of the active layer thickness. However, a lot of research work have proved that the charge collection efficiency of a device is inversely proportional to the square of the film thickness of the active layer.^[33,34] It was reflected in the decline of fill factor (FF) with the increase of film thickness. Also, the J_{sc} will decrease

due to the severe bimolecular recombination.^[35,36] Thus, it is still a challenge to obtain high efficiency devices with active layer thickness tolerance. To date, in the reported cases with active layer thickness tolerance, most are based on fullerene derivative acceptors and it has been found that the donor materials with high crystallinity and balanced mobility with fullerene derivative acceptors manifested better performance with high film thickness.^[35–38] Compared with fullerene derivatives based OSCs, it is much more challenging to realize thick-film NFAs OSCs with high performance since the electron mobilities of NFAs are usually lower than that of fullerene derivative acceptors.^[39,40] Thus, the charge transport and collection process in those NFA based thick films are not efficient. So far, great attentions have been drawn on the NFA based thick film OSCs and much progress have been made. For examples, Yip and co-workers reported devices based on PffBT4T-2OD:EH-IDTBR and realized a PCE of 9.1% with an active layer thickness of 300 nm by optimizing device architectures to overcome the space-charge effects.^[41] Zhang and co-workers reported devices based on PM6:IDIC with PCEs of 11.9% under the film thickness of 150 nm and 11.3% under the condition of 255 nm condition. Although the device performance is good enough, the cases with thicker active layers

Y. Zhang, H. Feng, L. Meng, Y. Wang, M. Chang, S. Li, Z. Guo, Prof. C. Li, Prof. X. Wan, Prof. Y. Chen
The Key Laboratory of Functional Polymer Materials
State Key Laboratory and Institute of Elemento-Organic Chemistry
Centre of Nanoscale Science and Technology
College of Chemistry
Nankai University
Tianjin 300071, China
E-mail: xjwan@nankai.edu.cn

Dr. N. Zheng, Prof. Z. Xie
State Key Laboratory of Luminescent Materials and Devices
South China University of Technology
Guangdong, Guangzhou 510640, P. R. China

The ORCID identification number(s) for the author(s) of this article can be found under <https://doi.org/10.1002/aenm.201902688>.

DOI: 10.1002/aenm.201902688

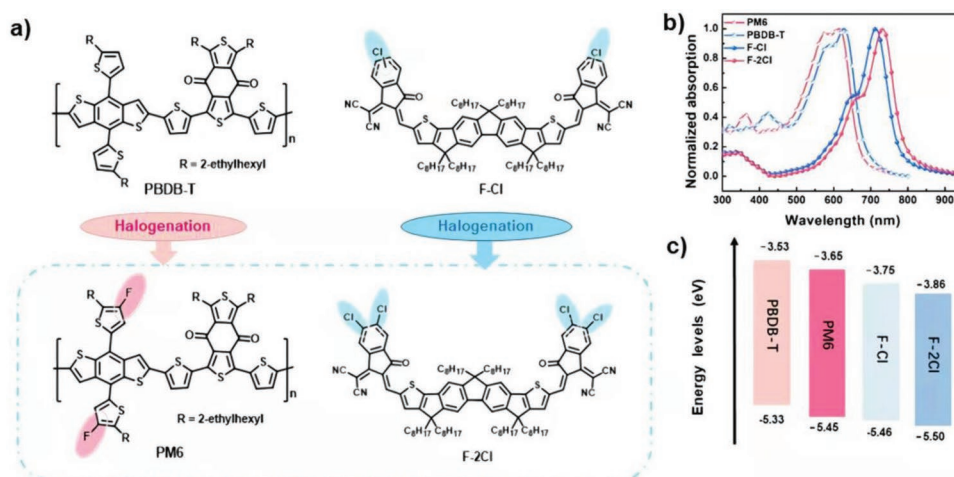


Figure 1. a) Chemical structures, b) film state UV–vis absorptions, and c) the energy level diagrams of PBDB-T, PM6, F–Cl, and F–2Cl.

were not mentioned.^[39] Recently, Yang and co-workers reported PTQ10:IDTPC based polymer solar cells which exhibited the optimized PCE of 12.2%, and gave a PCE of 10.0% with the active layer thickness of 400 nm. The main reason for the high performance in this case is that the hole and electron mobilities were relatively high with $\mu_{\text{h}}/\mu_{\text{e}}$ ratio of 0.90, which is beneficial to the charge transport in the devices.^[40] Therefore, designing NFAs with high electron mobilities and matched energy levels with donors might be an effective approach to obtain high performance thick-film devices.

Recently, we have reported a series of halogenated NFA molecules named F–F, F–Cl, and F–Br.^[42] Compared with that of the nonhalogenated molecule F–H,^[43] remarkable efficiencies with high FF were achieved for these three molecules based devices, which could attribute to the auxochromic effect of halogen atoms and high mobilities of those three molecules after halogenation. These results revealed that halogenation on the end-groups of NFAs has positive influences on increasing stacking order of these molecules. Therefore, another chlorine atom was introduced onto the end-group of F–Cl and a high halogen content acceptor named F–2Cl was synthesized (see chemical structure in **Figure 1a**) by our group.^[44] F–2Cl exhibits an obvious (010) diffraction peak in outofplane direction (OOP), and the π – π stacking distance is 0.04 Å smaller than that of F–Cl. In all small molecule devices we have reported recently, F–2Cl gave better device performance than F–Cl and F–H.^[44] These information demonstrated that F–2Cl has more compact packing thus higher crystallinity and potential in gaining higher performances in thick-film devices.

However, the introduction of the second chlorine atom inevitably further deepening the frontier molecular orbitals (FMOs) especially the lowest unoccupied molecular orbital (LUMO) of the acceptor F–2Cl. In comparison to F–Cl, the LUMO energy level of F–2Cl dropped 0.11 eV,^[44] which means if same polymer donor PBDB-T were utilized, the open circuit voltage (V_{oc}) of corresponding device will immensely decreased. Based on the above consideration, PM6 with two fluorine atoms on the conjugated side chains of BDT unit on PBDB-T was employed as donor material^[9,45,46] (Figure 1a). The halogenated polymer donor PM6 exhibits deeper highest occupied molecular orbital (HOMO) energy level, and have potential in compensating the

V_{oc} reduction caused by the halogenation of NFAs. For comparison, the devices based on PBDB-T:F–Cl, PBDB-T:F–2Cl, PM6:F–Cl, and PM6:F–2Cl were fabricated and the detailed photovoltaic performances were summarized in Table S1 in the Supporting Information. In line with our expectations, the device based on PM6:F–2Cl demonstrated the best performance among them with high PCEs of 12.83% in conventional device structure and 13.80% in inverted device structure. Furthermore, the hole and electron mobilities of PM6:F–2Cl were 3.79×10^{-4} and $2.83 \times 10^{-4} \text{ cm}^{-2} \text{ V}^{-1} \text{ s}^{-1}$ (Figure S2, Supporting Information), respectively. The $\mu_{\text{h}}/\mu_{\text{e}}$ is only 1.33, which is significantly lower than that of PBDB-T:F–Cl based device with $\mu_{\text{h}}/\mu_{\text{e}}$ value of 3.23. The higher mobilities and more balanced charge transport of PM6:F–2Cl indicated that the active layer with higher halogen contents might have better chance in achieving high efficiency under thick-film condition.

On account of different optical intensity distributions, the performances of inverted structure devices with different active layer thickness should be different from those of conventional structure devices,^[47] furthermore, the devices with inverted structures are more likely to gain better performances.^[48,49] Thus, the inverted devices based on PM6:F–2Cl with active layers of different thicknesses were fabricated and the detailed results are summarized in **Table 1**. As shown in Table 1 and **Figure 2b**, the J_{sc} s continuously increased and the FFs decreased along with the increase of film-thicknesses,

Table 1. Photovoltaic performance of the inverted structure solar cells based on PM6:F–2Cl blend films with different film thicknesses.

Thickness [nm]	V_{oc} [V]	J_{sc} [mA cm^{-2}]	$J_{\text{sc}}^{\text{cal}}$ [mA cm^{-2}]	FF	PCE _{max} [%]
60	0.893	18.30	17.43	0.78	12.90
100	0.891	19.52	18.33	0.78	13.53
120	0.893	19.74	19.09	0.78	13.80
200	0.879	19.94	19.26	0.68	11.93
250	0.867	20.00	20.86	0.60	10.51
350	0.866	19.73	20.18	0.58	10.00
500	0.852	19.78	19.99	0.53	9.03

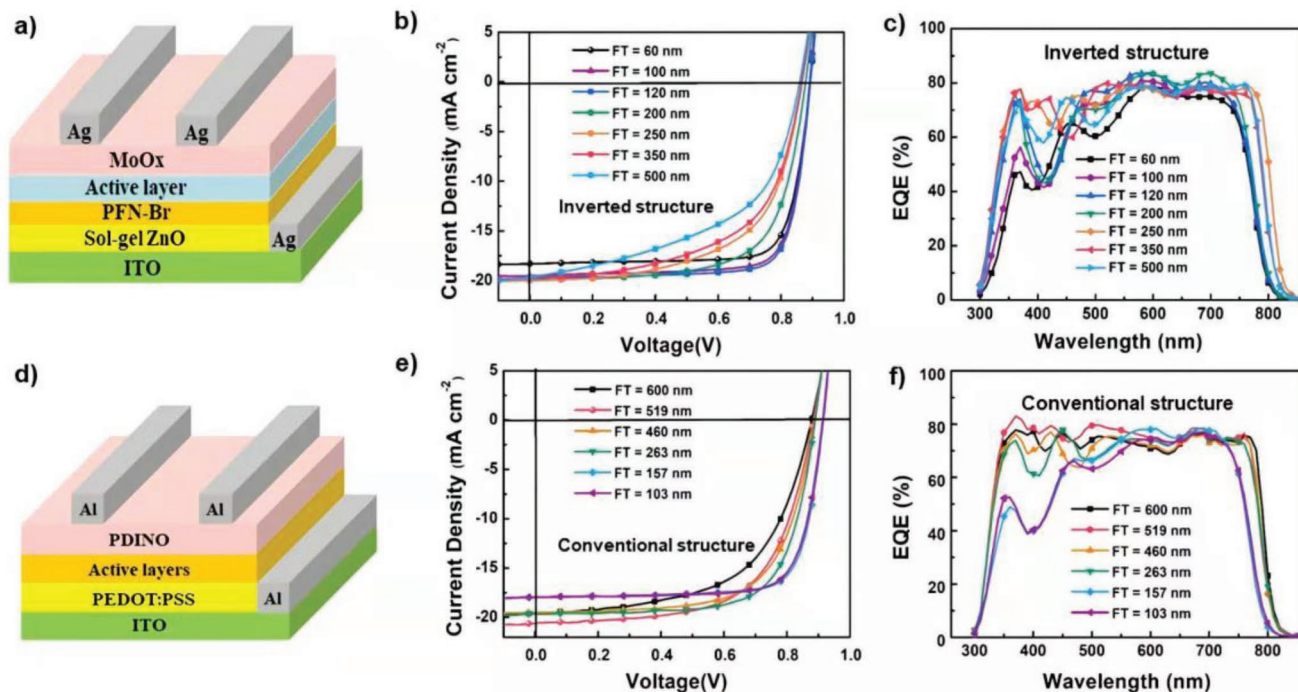


Figure 2. Device architecture of the a) inverted and d) conventional structure OSCs. The J - V curves of b) inverted and e) conventional structure devices with different film thicknesses. The EQE responses of c) inverted and f) conventional structure devices with different film thicknesses.

while the V_{oc} s declined from 0.893 to 0.852 V. The decrease of FFs and V_{oc} s in the thick-film devices is mainly caused by the more severe nongeminate recombination, which is consistent with the results of reported thick film devices.^[36,41] The optimal performance with high PCE of 13.80%, J_{sc} of 19.74 mA cm^{-2} and FF of 78.47% was obtained with the active layer thickness of 120 nm. When the film-thickness reached up to 350 nm, the J_{sc} started to descend, but high performance over 10% was still maintained. However, the drastically declined FFs in thick-film devices indicated that inefficient charge collection processes occurred so that the decreased PCE of 9.03% and low FF of 0.53 were obtained in the device with active layer thickness of 500 nm.

With the above consideration, the conventional structure devices with different active layer thicknesses were fabricated. As shown in Figure 2e and Table 2, the optimized device performance with conventional structure was obtained under the film-thickness at around 150 nm. Unlike the cases in inverted device structures, the J_{sc} s continuously increased until the

Table 2. Photovoltaic performance of the conventional structure solar cells based on PM6:F-2Cl blend films with different film thicknesses.

Thickness [nm]	V_{oc} [V]	J_{sc} [mA cm^{-2}]	J_{sc}^{cal} [mA cm^{-2}]	FF	PCE _{max} [%]
103	0.914	17.96	17.24	0.77	12.59
157	0.916	18.08	17.55	0.77	12.83
263	0.891	19.66	19.26	0.70	12.29
460	0.881	19.49	19.25	0.66	11.47
519	0.884	20.60	20.19	0.63	11.41
600	0.879	19.61	19.77	0.58	10.05

film-thickness reached 519 nm and the FFs decreased much slower, and the V_{oc} s slightly declined from 0.916 to 0.879 V. When the active layer thickness attained about 500 nm, the J_{sc} reached the ceiling value of 20.19 mA cm^{-2} . As shown in the external quantum efficiency (EQE) spectra (Figure 2f), the devices based on thick-films exhibited higher EQE responses in a wavelength range from 300 to 820 nm. Compared with the device with thinnest film of 103 nm, the device with highest J_{sc} (based on 519 nm-thick-film) showed 2.95 mA cm^{-2} enhancement in the J_{sc}^{cal} , and the response in the range from 300 to 550 nm significantly increased to 80%. When the film-thickness further increased to 600 nm, high PCE of 10.05% was still maintained.

The device parameters of different film-thickness devices in both conventional and inverted device structures were plotted together and shown in Figure 3a–d. In order to study the mechanism that cause the performance difference with the thick active layer films between the normal and inverted devices, we employed Auger electron spectroscopy-depth profiling analysis (AES-DPA) to investigate the vertical donor:acceptor (D:A) composition distributions in the BHJ films of these two structure devices. The elemental compositions of donor PM6 (represented by its monomer) are C (66.84%); H (6.43%); F (3.11%); O (2.62%); S (20.99%). For acceptor F-2Cl, the elemental compositions are C (74.02%); H (7.30%); Cl (9.01%); N (3.56%); O (2.03%); S (4.07%). The distributions of PM6 and F-2Cl could be tracked by detecting the distributions of fluorine atom and chlorine atom, respectively. Blending films with thicknesses of 400 nm were casted on two kind of substrates: poly(3,4-ethylenedioxythiophene):poly(styrenesulfonate) (PEDOT:PSS) for the conventional device and ZnO/PFN-Br for the inverted device. Then the films were etched with the

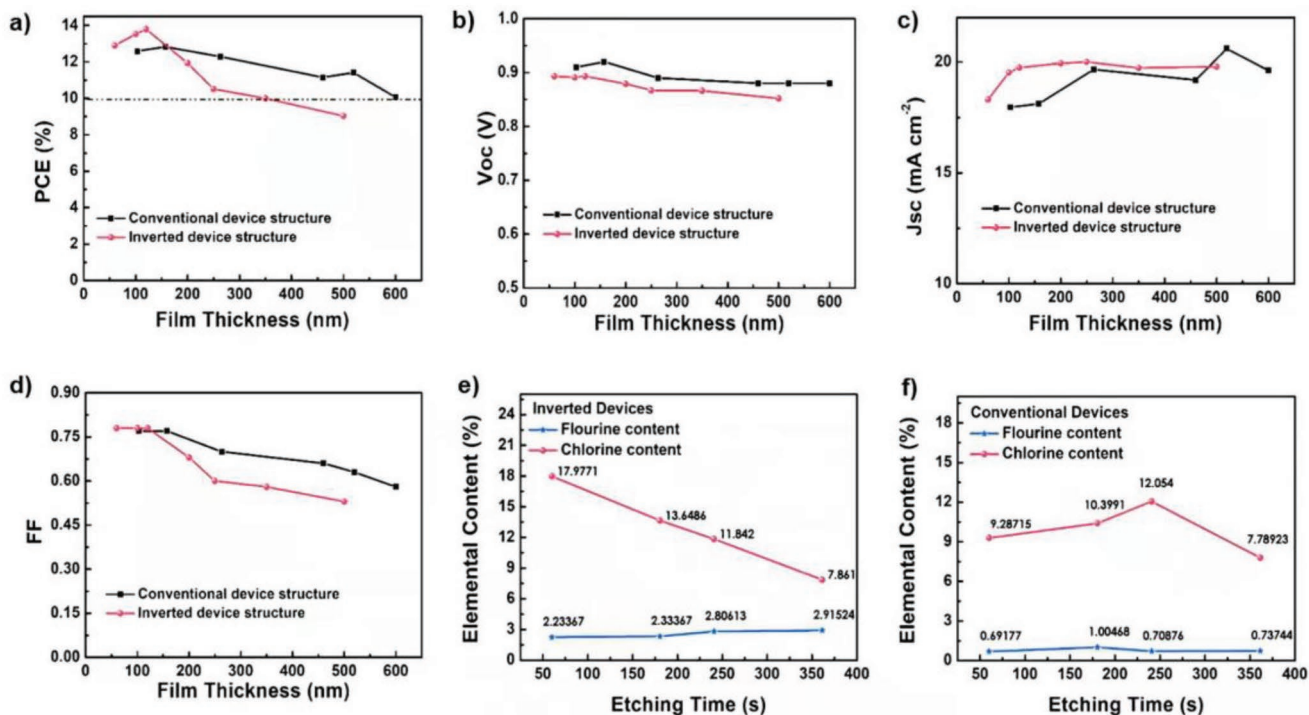


Figure 3. a–d) The device parameters of different film-thickness devices in both conventional and inverted device structures. The elemental content of chlorine and fluorine atoms use AES-DPA method in e) conventional and f) inverted structure devices (the elemental contents obtained in this measurement is based on an assumption that only F, Cl, O, C atoms are contained in the active layer, so the data in these figures are the relative value).

rate around 1 nm s^{-1} , and the signal of F (1s) and Cl (2p) were collected. As shown in Figure 3e, in the inverted structure devices, with the progressing of etching, the content of chlorine atoms is gradually decreasing, while the content of fluorine atom is slightly increasing, which indicate that the proportions of acceptor F–2Cl in the BHJ films are decreasing from the surface to the substrate. However, in the conventional structure devices, no significant changes were observed for the proportions of both donors and acceptors (Figure 3f). As is known, most of the incident light is absorbed near the transparent electrode side (the substrate), that means most of the excitons are generating and disassociating near this region.^[41] So in the inverted structure device with thick-film, the lower proportion of acceptor F–2Cl near the substrate region would restrict the electron transport and collection. In addition, the higher donor proportion in that region unavoidably results in longer transport distance of the holes. This undesirable vertical phase distribution in the inverted devices would lead to the decline of charge transport and collection efficiencies under thick film condition. However, the relatively equal distributions of donors and acceptors in the conventional structure device would not significantly influence the charge transport and collection processes either in thin or thick films. Therefore, the conventional structure thick-film devices obtained better PCEs under the thick-film condition. In addition, due to the close correlation between the vertical phase distribution and the process of charge generation and transport, the different vertical phase distributions in the normal and inverted devices will inevitably lead to the different shapes of their EQE curves (Figure 2c,f).

In order to further understand why the devices with normal structure could achieve higher efficiencies under high film-thicknesses, a series of characterizations were performed. As shown in Figure S4 in the Supporting Information, the UV–vis absorption intensities are in direct proportion to the film-thicknesses. The relative intensity of absorption peak at around 730 nm in contrast to the maxima absorption peak at 600 nm declined in the thick-film condition, indicating that the molecular packing between F–2Cl molecules decreased with the increase of active layer thickness, which might be one of the reasons for the drop of FFs. Morphological characterizations of active layers under different film-thicknesses were studied by tapping-mode atomic force microscopy (AFM) and transmission electron microscopy (TEM). As shown in the AFM height images (Figure S5, Supporting Information), thicker films exhibited slightly higher root-mean-square (rms) surface roughness values than those of thinner films, nevertheless, all the films showed uniform and smooth surface morphologies (Figure S6, Supporting Information). No obvious discrepancies can be observed from the TEM images (Figure S7, Supporting Information), indicating that there were almost no over-aggregated domains in the thick-film devices. GIWAXS were also used to investigate the intermolecular packing states of blend films with different thicknesses. As shown in Figure S8 in the Supporting Information, the neat film of PM6 and F–2Cl all exhibited faceon molecular packing with obvious (010) diffraction peaks in OOP direction at 1.71 and 1.86 \AA^{-1} , respectively, corresponding to π – π stacking distance of 3.67 and 3.37 \AA . After blended them together in different film-thicknesses, (010) diffraction peaks at 1.85 \AA^{-1} were observed in OOP direction

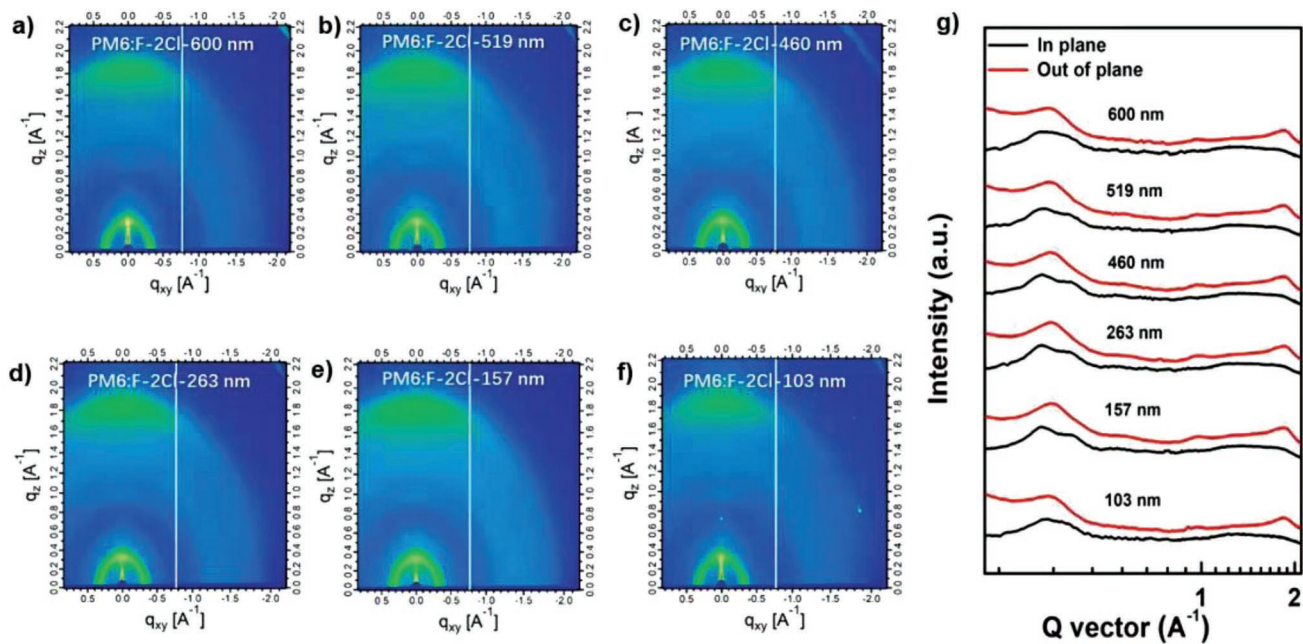


Figure 4. a–f) 2D GIWAXS patterns for PM6:F–2Cl blend films in the different film thicknesses. g) out-of-plane and in-plane GIWAXS profiles for these blend films.

for all the films. In addition, all of them demonstrated (100) diffraction peaks at 0.30 and 0.35 Å⁻¹, which can be assigned to the interchain packing of PM6 and F–2Cl, respectively. The similar diffraction peaks and intensities for blend films with different film-thicknesses reflected their similar intermolecular packing state, which is conducive to maintain the charge transport efficiencies in thick-films (**Figure 4**).

In summary, a high-halogen-content active layer has been designed to fabricate thick-film NFA based OSCs. The acceptor F–2Cl with halogenation of Cl significantly enhanced the electron mobility as well as broadened the absorption range. Meanwhile, the donor PM6 with halogenation of F efficiently compensated the V_{oc} reduction caused by the halogenation of F–2Cl and balanced the charge transport in the device. Both conventional and inverted structure devices with thick active layer films were fabricated. Different vertical donor:acceptor composition distributions in the BHJ films are found to be the principle reason for the different performance of these two structure devices. The higher performances obtained by the conventional thick-film devices could be attributed to the relatively equal distributions of donors and acceptors in its BHJ films. The devices with conventional structure maintained a PCE over 10% when the film-thickness is of 600 nm. To the best of our knowledge, it is the highest PCE value for NFA based devices with active layer thickness above 600 nm in the OSC field. The high efficiency with thick film tolerance make PM6:F–2Cl a promising candidate for the roll to roll application.

Experimental Section

Materials: The nonfullerene acceptors F–Cl and F–2Cl were synthesized according to the literatures^[41,43] All chemicals and solvents were reagent grades and purchased from Sigma-Aldrich, Alfa Aesar and

TCI Chemical Co. The polymer donor materials were purchased from Solarmer Materials Inc. PFN-Br was purchased from Luminescence Technology Corp. PDINO (perylene diimide functionalized with amino N-oxide) was purchased from Suna Tech Inc. All other materials were purchased and used as received.

Fabrication of Conventional Structure Device: The conventional devices were fabricated with the structure of indium tin oxide (ITO)/PEDOT:PSS(4083)/active layers/PDINO/Al (see Figure 2d). First, a thin layer (20 nm) of PEDOT:PSS was spin cast on top of precleaned ITO substrates and annealed in air at 150 °C for 15 min. Then PM6 and F–2Cl were dissolved in a mixed solvent of chlorobenzene/1,8-dioctane (99.7:0.3, v/v) with a weight ratio of 1:1. Different thicknesses were obtained by changing the concentration of the active layer solutions or the spinning rate. The film thicknesses were parallel tested by VeecoDektak 150 profilometer and Profilm3D model (no.: 205–0835). After that, about 5 nm PDINO (dissolved in methanol with the concentration of 1 mg mL⁻¹) layer was spin-coated on the top of the active layer. Finally, a layer of Al with thickness of 80 nm was deposited under high vacuum ($\approx 1 \times 10^{-4}$ Pa).

Fabrication of Inverted Structure Device: The inverted devices were fabricated with the structure of ITO/ZnO/PFN-Br/active layer/MoO_x/Ag (see Figure 2a). A layer of ZnO precursor was spin-coating on top of precleaned ITO substrates at 3000 rpm for 40 s followed by annealing at 200 °C for 1 h in air. Subsequently, a thin layer of PFN-Br was spin-coated on ZnO, then the substrates were transferred into glove box. The blend solution with different concentrations was spin-coated at different spinning rate to form the active layers. A layer of MoO₃ (6 nm) and a layer of Ag (70 nm) were then deposited on the active layer by vacuum evaporation under 2×10^{-4} Pa through a shadow mask. All the devices possess the work area of ≈ 0.04 cm².

Measurements and Instruments: UV–vis spectra were obtained with a JASCO V-570 spectrophotometer. Cyclic voltammetry (CV) experiments were performed with a LK98B II Microcomputer-based electrochemical analyzer in dichloromethane solutions. All measurements were carried out at room temperature with a conventional three-electrode configuration employing a glassy carbon electrode as the working electrode, a saturated calomel electrode (SCE) as the reference electrode, and a Pt wire as the counter electrode. Tetrabutyl ammonium

phosphorus hexafluoride (n-Bu₄NPF₆, 0.1 M) in dichloromethane was used as the supporting electrolyte, and the scan rate was 100 mV s⁻¹. The HOMO and LUMO energy levels were calculated from the onset oxidation potential and the onset reduction potential, using the equation $E_{\text{HOMO}} = -(4.80 + E_{\text{ox}}^{\text{onset}})$, $E_{\text{LUMO}} = -(4.80 + E_{\text{re}}^{\text{onset}})$. AFM investigation was performed using Bruker Multi Mode 8 in tapping mode. The TEM investigation was performed on Philips Technical G² F20 at 200 kV. The specimen for TEM measurement was prepared by spin casting the blend solution on ITO/PEDOT:PSS substrate, then floating the film on a water surface, and transferring to TEM grids. The hole and electron mobility were measured using the space charge limited current (SCLC) method, employing a diode configuration of ITO/PEDOT:PSS/active layer/Au for hole and glass/ZnO/active layer/Al for electron by taking the dark current density in the range of 0–8 V and fitting the results to a space charge limited form, where SCLC is described by

$$J = \frac{9\epsilon_0\epsilon_r\mu_0V^2}{8L^3} \exp\left(0.89\beta\sqrt{\frac{V}{L}}\right)$$

where J is the current density, L is the film thickness of the active layer, μ is the hole or electron mobility, ϵ_r is the relative dielectric constant of the transport medium, ϵ_0 is the permittivity of free space (8.85×10^{-12} F m⁻¹), V ($= V_{\text{appl}} - V_{\text{bi}}$) is the internal voltage in the device, where V_{appl} is the applied voltage to the device and V_{bi} is the built-in voltage due to the relative work function difference of the two electrodes. The Auger electron spectroscopy-depth analysis was performed on Thermo Fisher ESCALAB 250Xi-AER. The J - V characteristics of photovoltaic devices were obtained using a Keithley 2400 source-measure unit. Photocurrent was measured under illumination with simulated 100 mW cm⁻² AM 1.5G irradiation using a SAN-EI XES-70S1 AAA class solar simulator, calibrated with a reference Si solar cell. Simulator irradiance was characterized using a calibrated spectrometer and illumination intensity was set using a certified silicon diode without filter. The EQE spectrum was measured using a QE-R Solar Cell Spectral Response Measurement System (Enli Technology Co., Ltd., Taiwan).

Supporting Information

Supporting Information is available from the Wiley Online Library or from the author.

Acknowledgements

The authors gratefully acknowledge the financial support from MoST (2016YFA0200200) and NSFC (91633301, 21421001, 51873089, 51773095) of China, Tianjin city (17JCQJC44500, 17CZDJC31100) and 111 Project (B12015).

Conflict of Interest

The authors declare no conflict of interest.

Keywords

halogenation, nonfullerene acceptors, thick-film organic solar cells

Received: August 18, 2019

Revised: October 4, 2019

Published online:

[1] G. Li, R. Zhu, Y. Yang, *Nat. Photonics* **2012**, *6*, 153.

[2] N. S. Sariciftci, L. Smilowitz, A. J. Heeger, F. Wudl, *Science* **1992**, *258*, 1474.

- [3] C. W. Tang, *Appl. Phys. Lett.* **1986**, *48*, 183.
- [4] G. Yu, J. Gao, J. C. Hummelen, F. Wudl, A. J. Heeger, *Science* **1995**, *270*, 1789.
- [5] W. Zhao, S. Li, H. Yao, S. Zhang, Y. Zhang, B. Yang, J. Hou, *J. Am. Chem. Soc.* **2017**, *139*, 7148.
- [6] W. Li, S. Albrecht, L. Yang, S. Roland, J. R. Tumbleston, T. McAfee, L. Yan, M. A. Kelly, H. Ade, D. Neher, W. You, *J. Am. Chem. Soc.* **2014**, *136*, 15566.
- [7] Y. Lin, J. Wang, Z.-G. Zhang, H. Bai, Y. Li, D. Zhu, X. Zhan, *Adv. Mater.* **2015**, *27*, 1170.
- [8] Y. Liu, Z. Zhang, S. Feng, M. Li, L. Wu, R. Hou, X. Xu, X. Chen, Z. Bo, *J. Am. Chem. Soc.* **2017**, *139*, 3356.
- [9] M. Zhang, X. Guo, W. Ma, H. Ade, J. Hou, *Adv. Mater.* **2015**, *27*, 4655.
- [10] S. Zhang, Y. Qin, J. Zhu, J. Hou, *Adv. Mater.* **2018**, *30*, 1800868.
- [11] D. Qian, L. Ye, M. Zhang, Y. Liang, L. Li, Y. Huang, X. Guo, S. Zhang, Z. a. Tan, J. Hou, *Macromolecules* **2012**, *45*, 9611.
- [12] S. Dai, T. Li, W. Wang, Y. Xiao, T.-K. Lau, Z. Li, K. Liu, X. Lu, X. Zhan, *Adv. Mater.* **2018**, *30*, 1706571.
- [13] Z. Fei, F. D. Eisner, X. Jiao, M. Azzouzi, J. A. Röhr, Y. Han, M. Shahid, A. S. R. Chesman, C. D. Easton, C. R. McNeill, T. D. Anthopoulos, J. Nelson, M. Heeney, *Adv. Mater.* **2018**, *30*, 1705209.
- [14] X. Shi, J. Chen, K. Gao, L. Zuo, Z. Yao, F. Liu, J. Tang, A. K.-Y. Jen, *Adv. Energy Mater.* **2018**, *8*, 1702831.
- [15] C. Huang, X. Liao, K. Gao, L. Zuo, F. Lin, X. Shi, C.-Z. Li, H. Liu, X. Li, F. Liu, Y. Chen, H. Chen, A. K. Y. Jen, *Chem. Mater.* **2018**, *30*, 5429.
- [16] Y. Cui, H. Yao, L. Hong, T. Zhang, Y. Xu, K. Xian, B. Gao, J. Qin, J. Zhang, Z. Wei, J. Hou, *Adv. Mater.* **2019**, *31*, 1808356.
- [17] J. Yuan, Y. Zhang, L. Zhou, G. Zhang, H.-L. Yip, T.-K. Lau, X. Lu, C. Zhu, H. Peng, P. A. Johnson, M. Leclerc, Y. Cao, J. Ulanski, Y. Li, Y. Zou, *Joule* **2019**, *3*, 1140.
- [18] B. Fan, D. Zhang, M. Li, W. Zhong, Z. Zeng, L. Ying, F. Huang, Y. Cao, *Sci. China: Chem.* **2019**, *62*, 746.
- [19] Q. An, X. Ma, J. Gao, F. Zhang, *Sci. Bull.* **2019**, *64*, 504.
- [20] X. Xu, K. Feng, Z. Bi, W. Ma, G. Zhang, Q. Peng, *Adv. Mater.* **2019**, *31*, 1901872.
- [21] Y. Cui, H. Yao, J. Zhang, T. Zhang, Y. Wang, L. Hong, K. Xian, B. Xu, S. Zhang, J. Peng, Z. Wei, F. Gao, J. Hou, *Nat. Commun.* **2019**, *10*, 2515.
- [22] L. Meng, Y. Zhang, X. Wan, C. Li, X. Zhang, Y. Wang, X. Ke, Z. Xiao, L. Ding, R. Xia, H.-L. Yip, Y. Cao, Y. Chen, *Science* **2018**, *361*, 1094.
- [23] B. Kan, J. Zhang, F. Liu, X. Wan, C. Li, X. Ke, Y. Wang, H. Feng, Y. Zhang, G. Long, R. H. Friend, A. A. Bakulin, Y. Chen, *Adv. Mater.* **2018**, *30*, 1704904.
- [24] F. Zhao, S. Dai, Y. Wu, Q. Zhang, J. Wang, L. Jiang, Q. Ling, Z. Wei, W. Ma, W. You, C. Wang, X. Zhan, *Adv. Mater.* **2017**, *29*, 1700144.
- [25] J. A. Bartelt, D. Lam, T. M. Burke, S. M. Sweetnam, M. D. McGehee, *Adv. Energy Mater.* **2015**, *5*, 1500577.
- [26] B. Kan, M. Li, Q. Zhang, F. Liu, X. Wan, Y. Wang, W. Ni, G. Long, X. Yang, H. Feng, Y. Zuo, M. Zhang, F. Huang, Y. Cao, T. P. Russell, Y. Chen, *J. Am. Chem. Soc.* **2015**, *137*, 3886.
- [27] Y.-H. Chao, J.-F. Jheng, J.-S. Wu, K.-Y. Wu, H.-H. Peng, M.-C. Tsai, C.-L. Wang, Y.-N. Hsiao, C.-L. Wang, C.-Y. Lin, C.-S. Hsu, *Adv. Mater.* **2014**, *26*, 5205.
- [28] C. Cabanetos, A. El Labban, J. A. Bartelt, J. D. Douglas, W. R. Mateker, J. M. J. Fréchet, M. D. McGehee, P. M. Beaujuge, *J. Am. Chem. Soc.* **2013**, *135*, 4656.
- [29] D. Deng, Y. Zhang, J. Zhang, Z. Wang, L. Zhu, J. Fang, B. Xia, Z. Wang, K. Lu, W. Ma, Z. Wei, *Nat. Commun.* **2016**, *7*, 13740.
- [30] R. Søndergaard, M. Hösel, D. Angmo, T. T. Larsen-Olsen, F. C. Krebs, *Mater. Today* **2012**, *15*, 36.
- [31] *Laser Photonics Rev.* **2014**, *8*.
- [32] C. Duan, F. Huang, Y. Cao, *Polym. Chem.* **2015**, *6*, 8081.

- [33] B. W. Faughnan, R. S. Crandall, *Appl. Phys. Lett.* **1984**, *44*, 537.
- [34] T. Kirchartz, T. Agostinelli, M. Campoy-Quiles, W. Gong, J. Nelson, *J. Phys. Chem. Lett.* **2012**, *3*, 3470.
- [35] X. Liu, L. Nian, K. Gao, L. Zhang, L. Qing, Z. Wang, L. Ying, Z. Xie, Y. Ma, Y. Cao, F. Liu, J. Chen, *J. Mater. Chem. A* **2017**, *5*, 17619.
- [36] Y. Jin, Z. Chen, M. Xiao, J. Peng, B. Fan, L. Ying, G. Zhang, X.-F. Jiang, Q. Yin, Z. Liang, F. Huang, Y. Cao, *Adv. Energy Mater.* **2017**, *7*, 1700944.
- [37] D. Li, Z. Xiao, S. Wang, X. Geng, S. Yang, J. Fang, H. Yang, L. Ding, *Adv. Energy Mater.* **2018**, *8*, 1800397.
- [38] N. Gasparini, L. Lucera, M. Salvador, M. Prosa, G. D. Spyropoulos, P. Kubis, H.-J. Egelhaaf, C. J. Brabec, T. Ameri, *Energy Environ. Sci.* **2017**, *10*, 885.
- [39] Q. Fan, Y. Wang, M. Zhang, B. Wu, X. Guo, Y. Jiang, W. Li, B. Guo, C. Ye, W. Su, J. Fang, X. Ou, F. Liu, Z. Wei, T. C. Sum, T. P. Russell, Y. Li, *Adv. Mater.* **2018**, *30*, 1704546.
- [40] Z. Luo, C. Sun, S. Chen, Z.-G. Zhang, K. Wu, B. Qiu, C. Yang, Y. Li, C. Yang, *Adv. Energy Mater.* **2018**, *8*, 1800856.
- [41] G. Zhang, R. Xia, Z. Chen, J. Xiao, X. Zhao, S. Liu, H.-L. Yip, Y. Cao, *Adv. Energy Mater.* **2018**, *8*, 1801609.
- [42] Y. Wang, Y. Zhang, N. Qiu, H. Feng, H. Gao, B. Kan, Y. Ma, C. Li, X. Wan, Y. Chen, *Adv. Energy Mater.* **2018**, *8*, 1702870.
- [43] N. Qiu, H. Zhang, X. Wan, C. Li, X. Ke, H. Feng, B. Kan, H. Zhang, Q. Zhang, Y. Lu, Y. Chen, *Adv. Mater.* **2017**, *29*, 1604964.
- [44] Y. Wang, Y. Wang, B. Kan, X. Ke, X. Wan, C. Li, Y. Chen, *Adv. Energy Mater.* **2018**, *8*, 1802021.
- [45] H. Yao, F. Bai, H. Hu, L. Arunagiri, J. Zhang, Y. Chen, H. Yu, S. Chen, T. Liu, J. Y. L. Lai, Y. Zou, H. Ade, H. Yan, *ACS Energy Lett.* **2019**, *4*, 417.
- [46] L. Ye, S. Li, X. Liu, S. Zhang, M. Ghasemi, Y. Xiong, J. Hou, H. Ade, *Joule* **2019**, *3*, 443.
- [47] T. Kobori, T. Fukuda, *Org. Electron.* **2017**, *51*, 76.
- [48] Z. He, C. Zhong, S. Su, M. Xu, H. Wu, Y. Cao, *Nat. Photonics* **2012**, *6*, 591.
- [49] A. K. K. Kyaw, D. H. Wang, V. Gupta, J. Zhang, S. Chand, G. C. Bazan, A. J. Heeger, *Adv. Mater.* **2013**, *25*, 2397.